

# Three-Dimensional Charging via Multimode Resonant Cavity Enabled Wireless Power Transfer

Matthew J. Chabalko and Alanson P. Sample, *Member, IEEE*

**Abstract**—The majority of existing wireless power solutions are capable of 2-D surface charging of one or two devices, but are not well suited to deliver power efficiently to large numbers of devices placed throughout a large 3-D volume of space. In this paper, we propose an unexplored type of wireless power transfer system based on electromagnetic cavity resonance. Here, we use the natural electromagnetic modes of hollow metallic structures to produce uniform magnetic fields which can simultaneously power multiple small receiver coils contained almost anywhere inside. An analytical model is derived that predicts the coupling coefficient and power transfer efficiency from the cavity resonator to a small coil. These predictions are verified against simulated results with a coefficient of determination of 0.9943. By using two resonant modes, we demonstrate that a 3-in diameter receiver can be powered in nearly any location in a 140 cubic foot test chamber, at greater than 50% efficiency. Additionally, we show that ten receivers can be powered simultaneously and that this system is capable of recharging consumer electronics such as a cell phone.

**Index Terms**—Cavity resonator, multimode, wireless power, 3-D charging.

## I. INTRODUCTION

WIRELESS power transfer has the potential to enable many new applications in the industrial, scientific, and medical fields where innovative solutions are limited by the requirements for wired connections to provide system power and battery charging [1], [2]. The challenge for wireless power systems is to provide highly efficient power transfer to large regions of space, thus enabling device charging in an unencumbered and seamless fashion. Consider the challenge of recharging medical devices such as hearing aids that are too small to hold, swarms of 100–1000s of miniature robots that are too numerous to maintain, and industrial tools that are bulky and oddly shaped [3]. Scenarios such as these require wireless power systems to provide enough geometric freedom so that the user can simply place their devices in a recharging zone without the need for precise positioning and/or alignment. Part of this geometric freedom means that wireless power systems need to effectively deliver power to 3-D volumes of space rather than just small 2-D surfaces. Additionally, as multiple devices are added, the wireless power system should be able to scale seamlessly while maintaining high transfer efficiency to all devices.

There are a wide variety of wireless power techniques that meet many of these challenges, each with their unique strengths

Manuscript received October 14, 2014; accepted May 18, 2015. Date of publication June 8, 2015; date of current version July 10, 2015. Recommended for publication by Associate Editor Y. J. Jang.

The authors are with Disney Research, Pittsburgh, PA 15213 USA (e-mail: matt.chabalko@disneyresearch.com; alanson.sample@disneyresearch.com).

Color versions of one or more of the figures in this paper are available online at <http://ieeexplore.ieee.org>.

Digital Object Identifier 10.1109/TPEL.2015.2440914

and weaknesses. Traditional inductive charging systems have long been used for applications like rechargeable toothbrushes and achieve good power transfer efficiency without the need for complex electronics. However, inductive systems require cradles and/or permanent magnets for alignment and are effectively limited to charging a 1-D point in space [4].

Alternatively, magnetoquasistatic (MQS) wireless power techniques provide greater geometric freedom when operating in the overcoupled regime. Proper tuning allows for misalignment tolerance between the transmitter and receiver [5] while maintaining high power transfer efficiency. Transfer distance is also improved, but efficiency drops off rapidly once the receiver is moved approximately one coil diameter from the transmitter [6]–[9]. Generally speaking, these types of solutions are well suited for “charging pad” [10], [11] scenarios where one or two small receivers are placed on a 2-D charging surface.

Far-field wireless power transfer methods provide the most spatial freedom, but there is an inherent tradeoff between providing efficient power transfer to one device versus providing power to many devices at once. For example, an ultrahigh frequency radio-frequency identification (RFID) reader can power hundreds of RFID tags simultaneously in a large room, but the transfer efficiency is less than 0.01%. Alternatively, beam-forming techniques can achieve very high transfer efficiency to one device at a time ( $\sim 80\%$ ), but require sophisticated tracking and alignment mechanisms [12]–[14].

In this paper, we propose an unexplored form of wireless power that can provide efficient power delivery to nearly all locations in a confined 3-D volume of space. This is accomplished by stimulating the natural electromagnetic resonant modes of a metallic structure with low-level electromagnetic fields, so that energy can be efficiently coupled to small receivers placed within the structure. An example application is depicted in Fig. 1(a), which shows a metallic toy chest filled with electronic toys and devices. In this scenario, toys with small coil receivers can be placed in the box in a random and overlapping fashion. Panel (b) shows the field distribution of one of the electromagnetic modes when the toy chest is closed. By using one or more resonant modes of the cavity, 10s to 100s of receivers can be powered in nearly any orientation and/or position as long as strong coupling between the cavity mode field and receiver is achieved. To the best of our knowledge, this particular form of wireless power delivery has not previously been reported in the literature.

In this paper, an investigation of cavity mode enabled WPT is presented, and it is shown that it is possible to deliver wireless power to large portions of the 3-D space at high efficiency. It expands on the initial results we presented in [15], which focused mainly on analytic and experimental determination of the coupling coefficient. In Section II, an expression for the coupling

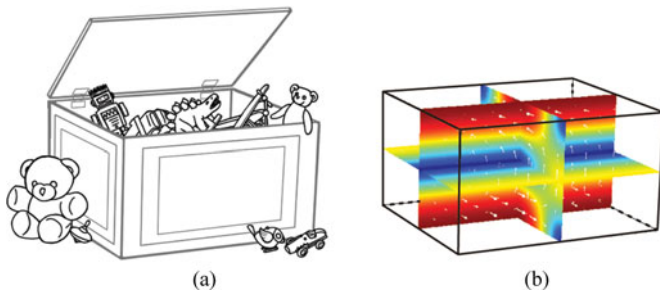


Fig. 1. (a) Illustration depicting an application of cavity mode enabled WPT where multiple toys in a toy chest are recharged. (b) Example field pattern of a mode of a cavity resonator. White arrows are magnetic flux density vectors, and color is magnitude of the magnetic flux density (Red, large; Blue, small). The cavity mode fields couple to receivers installed in the toys and provide power wirelessly.

coefficient between the chamber and a receiver is derived, and the results are used to predict expected WPT efficiency. Next, in Section III, the experimental setup is described, which consists of a large test chamber, and measured results are presented for power transfer to a small 3-in receiver. These measured results are compared with the analytical model, and it is shown that, using two resonant modes, a device can be powered nearly anywhere within the 140 cubic foot volume of the test chamber. Finally in Section IV, ten receivers are simultaneously powered wirelessly, and finally, the recharging of a cellular phone is also demonstrated.

## II. THEORY OF OPERATION AND ANALYTICAL MODELING

In this section, the underlining physics of cavity mode enabled WPT is presented. This begins with a conceptual discussion describing the operating principles of using electromagnetic cavity resonance to transfer power to a receiver. Then, a rigorous analysis is performed using coupled mode theory (CMT) to derive an expression for the coupling coefficient between a cavity and a small receiver as a function of receiver location. The results of this analytical expression for the coupling coefficient are compared to finite-element method (FEM) simulations and show good agreement. Finally, the expression for the coupling coefficient is expanded to predict the wireless power transfer efficiency to a receiver placed anywhere inside the cavity.

### A. System Overview

Traditionally, electromagnetic cavity resonators have been used in microwave filters where they operate in a similar manner to waveguides [16]. In this paper, the cavity resonator has been reinterpreted as a general-purpose method for generating uniform standing electromagnetic waves in an enclosed structure, which can be used to power small receivers contained within. Fig. 2 shows a conceptual diagram of a cavity resonator consisting of metallic walls, along with the field distributions of two of the cavity's resonant modes in panels (b) and (c). The mechanism for exciting these electromagnetic standing waves is similar to how a mechanical standing wave can be imposed on a guitar string, or how a 3-D pressure wave can be produced in a drum.

The key insight is that the field distribution is defined by the boundary conditions of the resonant structure and by choosing the proper frequency that stimulates different resonant modes. For example, consider the standing pressure and velocity waves in air produced inside a bass drum cavity when the diaphragm is struck. Here, the diaphragm launches pressure waves that reverberate off the inside walls of the drum cavity, producing a tone. This tone is defined by the shape (diameter and height) of the drum cavity but also by the frequency of the oscillating diaphragm. Higher order modes (i.e., higher tones) can be produced in the same drum by hitting the diaphragm in different places (i.e., on the edge of the diaphragm). In this study, it is not standing pressure waves that are formed, but instead uniform standing electromagnetic fields are formed as RF waves reflect off the inside of the walls of the metallic cavity. These fields produce well-defined structures [as seen in Fig. 2(b) and (c)], which can be used to transfer wireless power to a receiver located nearly anywhere inside. Although electromagnetic resonant modes exist for nearly any arbitrarily shaped and confined vessel, for the purposes of this investigation, we focus on rectangular structures.

Wireless power receivers can consist of any of the traditional coil shapes from planar spirals to helical solenoids. Here, the magnetic fields of the aforementioned cavity modes are used to induce currents in small closed-loop receivers. Since the magnetic fields of resonant cavity modes possess high spatial uniformity, using a combination of resonant modes enables high-efficiency WPT regardless of the receiver's position or orientation within the cavity resonator. This is as opposed to inductive and resonant WPT systems where the toroidal-shaped magnetic field generated by coil transmitters drops off rapidly as distance increases, resulting in applications with limited range (i.e., 2-D surface and 1-D point charging).

In this study, the theoretical and experimental analyses are done for the  $TE_{011}$  and  $TE_{012}$  modes, which are characteristic electromagnetic eigenmodes of the cavity resonator. These particular modes are inherent to *any* rectangular cavity resonator. Physically, they result from the resonance created between the electric and magnetic fields as standing electromagnetic waves form within the cavity due to the superposition of waves traveling toward the cavity walls and then reflecting off of the interior metallic walls of the cavity. The "TE" refers to transverse electric fields and the subscript  $m, n, p$  as in  $TE_{mnp}$  refer to the number of antinodes in the electric field in the  $x$ -,  $y$ -, and  $z$ - directions, respectively. Higher  $m$ ,  $n$ , and  $p$  typically yield higher resonant frequencies, so a designer should bear in mind the operating frequency range when designing the size of the cavity (size also affects resonant frequency). Additionally, it is also important for a designer to consider which modes are necessary to deliver power to receivers as envisioned in a particular application. A more detailed analysis of the mathematics and physical origins of electromagnetic cavity modes can be found in [16]–[18].

Finally, for any system that transfers energy via the coupling of resonant modes, the fundamental parameters are: the coupling coefficient between the source and receiver resonators, the quality factors ( $Q$ -factors) of each resonator, and the resonant frequency of the coupled system [6], [19]. For the system described in this study, the quality factor for both a cavity

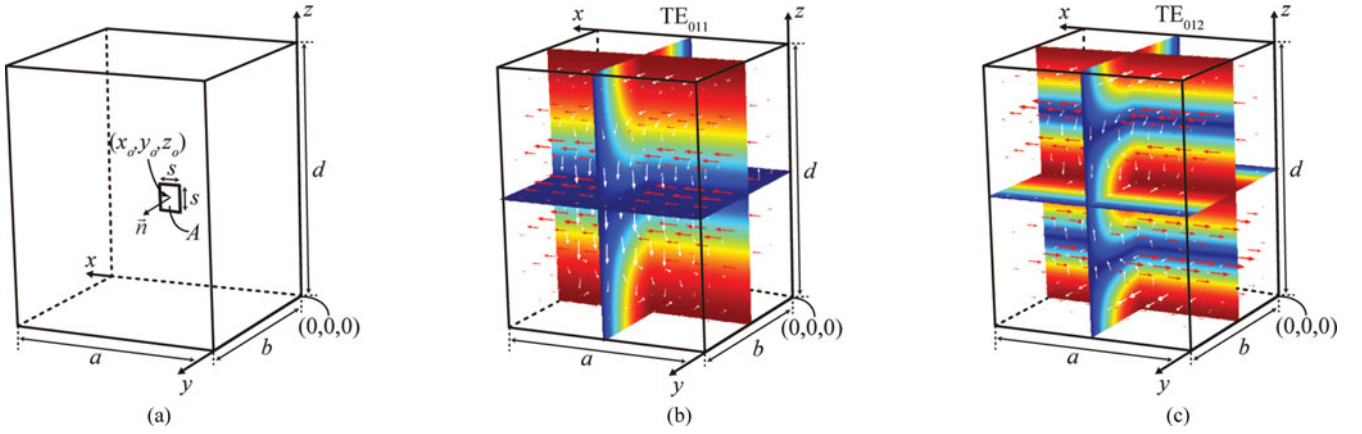


Fig. 2. (a) Diagram of the rectangular cavity resonator used in this study. A single-turn square-shaped receiver with side length,  $s$ , lying flat in the  $xz$  plane is used throughout this study, centered at  $(x, y, z) = (x_o, y_o, z_o)$ . Panels (b) and (c) are the simulated fields of the (b)  $TE_{011}$  and (c)  $TE_{012}$  for a cavity with the same dimensions as the experimental cavity used in this study. Color:  $y$ -component of the magnetic flux density,  $|B_y|$ : Red, large; Blue, small. Red arrows:  $\vec{E}$ -field vectors. White arrows:  $\vec{B}$ -field vectors.

resonator and coil receiver can each be independently found in the literature [6], [16]. In the next section, we derive an expression for the coupling coefficient,  $\kappa$  between a rectangular cavity resonator and a square, single-turn coil receiver using CMT. Once  $\kappa$  is found, it can be used to calculate the efficiencies of WPT that can be expected, based solely on the system's geometry and material properties. The resonant frequency of the coupled system is defined once a particular cavity mode has been selected (for example, the transverse electric  $TE_{011}$  mode).

### B. Derivation of the Coupling Coefficient

In this section, a cavity with dimensions  $a \times b \times d$ , containing a square shaped receiver with side length  $s$ , centered at position  $(x_o, y_o, z_o)$  will be analyzed [see Fig. 2(a)]. To begin the derivation of the coupling coefficient between the cavity and receiver coil, standard CMT is employed as it enables analysis of *any* coupled resonator systems. This is opposed to circuit theory, which does not take into account the shape and variation of the electromagnetic field distributions. In CMT, a differential equation is used to describe the coupling of two generic lossless resonators as a function of time. Below, this general analysis will be extrapolated to analyze the specific case of the coupling between a cavity resonator and a coil receiver. First, each resonator is defined to have a resonant frequency and amplitude,  $\omega_1, a_1$  and  $\omega_2, a_2$  (with  $\omega_{1,2} = 2\pi f_{1,2}$ ), respectively, and that, using phasor notation, they have the time dependence  $\exp(j\omega_{1,2}t)$ . Thus, standard CMT is used to write the differential equations that describe the coupled resonators' amplitude evolution over time [20], [21]

$$\begin{aligned} \frac{d}{dt}a_1 &= j\omega_1 a_1 + j\kappa_{12}a_2 \\ \frac{d}{dt}a_2 &= j\omega_2 a_2 + j\kappa_{21}a_1 \end{aligned} \quad (1)$$

where  $\kappa_{12} = \kappa_{21}^* \triangleq \kappa$  is the coupling coefficient between the two resonators and  $*$  indicates the complex conjugate. It should

be noted that “kappa”  $\kappa$  is not the same the coupling coefficient,  $k$ , commonly used in MQS WPT analysis (i.e.,  $M = k\sqrt{L_1 L_2}$ ). To conform to standard CMT,  $a_{1,2}$  is defined as having stored energy of  $\text{Energy} = |a_{1,2}|^2$ . A review of the literature on CMT and derivations of the coupling coefficient for various systems makes it clear that use of energy conservation arguments [19]–[21] is a typical approach to employ in deriving the coupling coefficient. In following this general methodology, note that the power fed from resonator one into resonator two,  $P_{21}$ , must be equal to the time rate of change of energy in resonator two. Mathematically, this is written as

$$P_{21} = \frac{d}{dt}|a_2|^2. \quad (2)$$

To evaluate the above expression, it is helpful to note that  $|a_2|^2 = a_2 a_2^*$ . Thus, by first using the product rule for derivatives on the right-hand side of  $|a_2|^2 = a_2 a_2^*$ ,  $a_2$  and  $a_2^*$  can be each inserted into (1), and the results used to obtain an expression for  $P_{21}$ , which will explicitly contain the coupling coefficient [21]

$$P_{21} = \frac{d}{dt}|a_2|^2 = j\kappa a_1 a_2^* - j\kappa^* a_1^* a_2. \quad (3)$$

In (3),  $\kappa$  can be solved for when  $P_{21}$  and  $a_{1,2}$  are known. The task, now, becomes evaluating this expression for the specific cavity-to-coil coupled mode system; the methodology is the same, but is now specific to the physical architecture of the enclosed space. Again, it becomes necessary to obtain an expression for  $P_{21}$ —the power flowing from *resonator-one* (the resonant cavity mode) into *resonator-two* (the square loop receiver with capacitor to form an  $LC$  resonator). Since the receiver is a coil/inductor, the treatment here will neglect the coupling via the electric field, and only consider the coupling of the cavity to the coil via the magnetic fields of the resonant cavity mode. Using analysis similar to that in [19], the power flowing from the chamber to the coil in terms of the magnetic fluxes crossing

the surface of the receiver loop can be written as

$$P_{21} = i_2 \frac{d(\phi_1 - \phi_2)}{dt} = \frac{\phi_2}{L_2} \frac{d(\phi_1 - \phi_2)}{dt} \quad (4)$$

where  $\phi_1$  is the instantaneous total normal flux—due to the resonant cavity mode's magnetic fields—crossing the coil's surface,  $A$  [see Fig. 2(a)]. Similarly,  $\phi_2$  is the instantaneous time-dependent flux crossing the coil's surface,  $A$ , due to the fields generated by a current,  $i_2$ , in the coil. In the rightmost expression in (4), a substitution is made using the usual relation  $\phi_2 = L_2 i_2$ , where  $L_2$  is the inductance of the receiver coil. Explicit evaluation of  $\phi_1$ , which relates to the magnetic field patterns of any particular cavity mode, will be done later on for clarity of presentation.

Next,  $\phi_{1,2}$  is reformulated in terms of  $\Phi_{1,2}$ , which are the time-dependent complex envelope functions of the fluxes

$$\phi_{1,2}(t) = \frac{\Phi_{1,2} e^{j\omega_{1,2}t} + \Phi_{1,2}^* e^{-j\omega_{1,2}t}}{2}. \quad (5)$$

Then, substituting (5), into (4), and simplifying the result by assuming that the  $\frac{d}{dt}\Phi_{1,2}$  terms are small compared to the  $j\omega\Phi_{1,2}$  terms such that  $\frac{d}{dt}\Phi_{1,2}$  can be neglected, results in

$$P_{21} = \frac{1}{4L_2} \left( j\omega_1 \Phi_1 e^{j\omega_1 t} \Phi_2^* e^{-j\omega_2 t} - j\omega_1 \Phi_1^* e^{-j\omega_1 t} \Phi_2 e^{j\omega_2 t} \right). \quad (6)$$

A comparison of the above in (6) reveals that it is similar to the form of (3). The only difference is that currently (6) is written in terms of  $\Phi_{1,2}$  instead of  $a_{1,2}$ . Thus, what is desired is to make appropriate substitutions such that  $\Phi_{1,2}$  terms can be replaced with  $a_{1,2}$  terms:  $\Phi_{1,2} \rightarrow a_{1,2}$ , in (6). After that, some algebraic manipulation is used to write (6) to match the form of (3) and permit identification of  $\kappa$ .

To make this substitution, recall that it was necessary for the total energy stored in resonator one and two to be  $|a_{1,2}|^2$ , as was defined in (1) and (3). To write  $a_{1,2}$  in accordance with this requirement, three parameters are essential:  $\alpha$ , the total magnetic energy stored in the chamber,  $\beta$  the total flux crossing the receiver's surface due to the chamber's modal magnetic fields,  $\vec{H}$ , and  $\zeta$ , a constant relating to the energy stored in the coil  $LC$  resonator. These parameters can be evaluated using the following expressions:

$$\alpha = \iiint_V \frac{\mu_o}{2} |\vec{H}|^2 dV \quad (7)$$

$$\beta = \iint_A \mu_o \vec{H} \cdot \vec{n} dA \quad (8)$$

$$\zeta = \frac{1}{\sqrt{2L_2}}. \quad (9)$$

Here,  $V$  is the volume of the chamber, and  $\vec{n}$  is the unit normal vector of the coil's surface [as in Fig. 2(a)] and  $\mu_o$  is the permeability of free space (assuming an air filled chamber). Using these parameters and some algebraic manipulation,  $a_{1,2}$  can be normalized such that  $|a_1|^2$  is the total magnetic energy

stored in *resonator-one* (the cavity mode), and  $|a_2|^2$  is the total energy stored in *resonator-two* (the  $LC$  tank formed by the coil and capacitor). The explicit expressions for  $a_{1,2}$  are

$$a_1 = \Phi_1 \frac{\alpha^{1/2}}{\beta} e^{j\omega_1 t}, \quad a_2 = \Phi_2 \zeta e^{j\omega_2 t}. \quad (10)$$

After writing  $a_{1,2}$  as in (10), they fit the framework of CMT, such that it is possible substitute (10) into (6)

$$P_{21} = \left( j \frac{\omega_1}{4L_2} \frac{\beta}{\alpha^{1/2}} \frac{1}{\zeta} a_1 a_2^* - j \frac{\omega_1}{4L_2} \frac{\beta}{\alpha^{1/2}} \frac{1}{\zeta} a_1^* a_2 \right). \quad (11)$$

Then, (11) is the same form as (3), and a comparison of coefficients between (11) and (3) yields the coupling coefficient

$$\kappa = \frac{1}{4} \frac{\omega_1 \beta}{L_2 \alpha^{1/2} \zeta} = \frac{\sqrt{2}}{4} \frac{\omega_1 \beta}{\sqrt{L_2} \alpha}. \quad (12)$$

Finally, it should be noted that the preceding analysis assumes the resonant frequency of the chamber is the same as the receiver, i.e.,  $\omega_1 = \omega_2$ . This expression can be used to evaluate the coupling coefficient between *any* cavity mode and a small closed-loop receiver.

As an example of how to compute the coupling coefficient, the  $TE_{012}$  mode will be used here since it has regions of relatively high magnetic flux density near the middle of the chamber, which is a common place to put one or more receivers. A plot of the  $TE_{012}$  mode's field distribution is shown in Fig. 2(c), as simulated using the commercial FEM-based software COMSOL Multiphysics. In particular, it can be seen that the magnetic flux is largely  $y$ -directed near the center of the chamber. Thus, the studies in this paper will concentrate on receiver coils that lie in the  $xz$  plane (i.e.,  $\vec{n} = \vec{a}_y$ ). If, for example, the receiver instead lies in the  $yz$  plane, the  $TE_{101}$  mode could be used. By symmetry of the rectangular cavity, this  $TE_{101}$  mode generates  $x$ -directed flux as opposed to the  $y$ -directed flux of the  $TE_{011}$ . The distinction between modes is made by use of the  $m, n, p$  convention and the fixed coordinate system. Returning now to the  $TE_{012}$  mode, and with reference to the coordinate system in Fig. 2, the  $y$  and  $z$  components of the magnetic field,  $H_y$  and  $H_z$ , respectively, within the chamber can be written as [22]

$$H_z = A_o \cos\left(\frac{\pi y}{b}\right) \sin\left(\frac{2\pi z}{d}\right) \quad (13)$$

$$H_y = A_o \frac{k_y k_z}{k_o^2 - k_z^2} \sin\left(\frac{\pi y}{b}\right) \cos\left(\frac{2\pi z}{d}\right) \quad (14)$$

where  $A_o$  is the peak value of the  $z$ -directed magnetic field, and  $a$ ,  $b$ , and  $d$ , are the length, width, and height of the cavity, respectively, as in Fig. 2.  $k_y$ ,  $k_z$ , and  $k_o$  are the  $y$ -component,  $z$ -component, and norm of the wave vector of the standing wave within the cavity, respectively. They are given by

$$k_y = \frac{\pi}{b}, \quad k_z = \frac{2\pi}{d}, \quad k_o = \sqrt{\left(\frac{\pi}{b}\right)^2 + \left(\frac{2\pi}{d}\right)^2}. \quad (15)$$

Once the  $\vec{H}$ -field components are obtained, (7) and (8) can be used to compute  $\alpha$  and  $\beta$ . In this case, (7) can be evaluated to

find the magnetic energy stored in the chamber

$$\alpha = \frac{A_o^2 \mu_o ab (4b^2 + d^2)}{8d}. \quad (16)$$

In this example, the receiver lies flat in the  $xz$  plane and will only couple to the  $y$ -component of the cavity's magnetic field, which will be reflected in later plots of  $\kappa$ . The plots will reveal that  $\kappa$  is relatively large or small wherever  $B_y = \mu_o H_y$  is large or small. Thus, evaluating (8) for a square-shaped coil with side length  $s$ , unit normal  $\vec{n} = \vec{a}_y$ , and inductance  $L_2$ , centered at position  $(x_o, y_o, z_o)$ , the magnetic flux coupled from the chamber to the coil is

$$\beta = \frac{2A_o \mu_o b s}{\pi} \sin\left(\frac{\pi y_o}{b}\right) \sin\left(\frac{\pi s}{d}\right) \left(2 \cos^2\left(\frac{\pi z_o}{d}\right) - 1\right). \quad (17)$$

Finally,  $\kappa$  can be determined for the  $TE_{012}$  mode by substituting (16) and (17) into (12)

$$\kappa = \frac{\sqrt{16}\omega_1 b s \mu_o \sin\left(\frac{\pi y_o}{b}\right) \sin\left(\frac{\pi s}{d}\right) \left(\cos^2\left(\frac{\pi z_o}{d}\right) - \frac{1}{2}\right)}{\sqrt{L_2} \pi \sqrt{\frac{\mu_o ab(4b^2 + d^2)}{d}}}. \quad (18)$$

For this example, the coupling coefficient does not depend on the coil's  $x$ -position because the modal fields do not vary in the  $x$ -direction (as seen from the 0 in  $TE_{012}$ ), but other modes that do have variation in their magnetic flux with  $x$  would likewise show variation in the coupling coefficient as the  $x$ -location of the receiver changes.

### C. Analytical Model Compared to FEM Simulation

In order to determine the accuracy of the analytically derived expression for  $\kappa$ , COMSOL FEM simulations were performed for comparison. To do this, a cavity resonator was simulated with dimensions  $a = 1.52$  m,  $b = 1.42$  m, and  $d = 1.83$  m, along with a square-shaped receiver placed inside with a side length of 7.62 cm, lying in the  $xz$  plane (as in shown Fig. 2). The study of the coupling coefficient  $\kappa$  was performed for the  $TE_{012}$  mode, while the simulated receiver was moved across the  $xy$  plane at a height  $z_o$  of  $d/2 = 91$  cm. The analytically predicted  $\kappa$  and simulated  $\kappa$  are shown in Fig. 3(a) and (b). A line slice plot comparing analytic and simulated coupling coefficients across a single  $x$ -slice is shown in Fig. 3(c). When compared to the simulated COMSOL data, the analytical model has an average coefficient of determination ( $R^2$ ) of 0.9943, where an  $R^2$  of 1 indicates that the model perfectly predicts the outcome. This indicates with high confidence that the analytic model can predict the coupling coefficient. Additionally, the raw error between FEM simulation and analytic model at any point in the plot of Fig. 3(c) is less than 5%.

### D. Calculating WPT Efficiency

Obtaining an analytical expression for  $\kappa$  is important since it is one of the key parameters needed to determine the transfer efficiency of the cavity-to-coil WPT system. The other important parameters are the  $Q$ -factors of the cavity and receiver loop resonator. The expression for the maximum possible WPT efficiency,  $\eta_{\max}$ , of a coupled resonator system is described in [6]

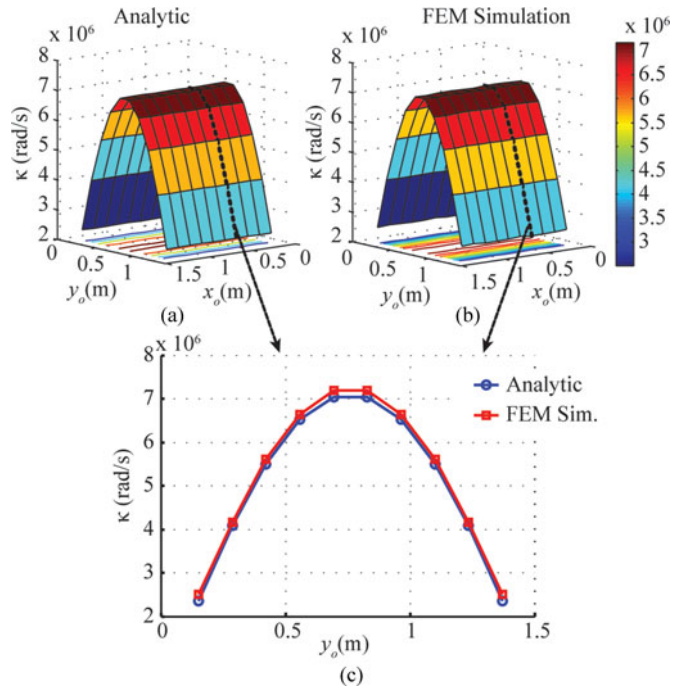


Fig. 3. (a) Analytic coupling coefficient,  $\kappa$  over an  $x$ - $y$  plane at a  $z$ -height of 0.91 m between the  $TE_{012}$  mode of the chamber and a square shaped receiver. (b) COMSOL FEM simulated  $\kappa$  over the same plane. (c) Lineslice comparing the two directly. The bold dotted lines in (a) and (b) are the lineslices plotted in (c). The  $R^2$  correlation coefficient between (a) and (b) is 0.9943.

and can be rewritten as

$$\eta_{\max} = \frac{\chi}{(1 + \sqrt{1 + \chi})^2} \quad (19)$$

$$\chi = \frac{4Q_1 Q_2 |\kappa|^2}{\omega_1 \omega_2}.$$

Therefore, given the  $Q$ -factors of the chamber and the receiver coil, along with the coupling coefficient between the two resonators, and the resonant frequencies of the two resonators, it is possible to predict an upper bound on the WPT efficiency at any point in the cavity. In the literature, this quantity is often referred to as the maximum available gain ( $G_{\text{mag}}$ ) [23] and is the maximum possible power gain between the input and output ports of a two-port network. Stated another way, this is the power gain when the two port network is biconjugate matched using a *lossless* impedance matching network.

In this study,  $\eta_{\max}$  is used as the figure of merit for how well cavity mode enabled WPT can perform and gives an appreciation for the potential system performance.  $\eta_{\max}$  only depends on the cavity mode enabled WPT link, and not the impedance-matching network used to gain achieve efficiency. In this way, the effect of impedance matching network losses is controlled for, where in calculation of  $\eta_{\max}$  they are assumed to be zero.

Finally, note that (19) is essentially the same as the more familiar expression in [24], and  $\chi$  reduces to  $\chi = (\omega M)^2 / R_1 / R_2$  for two resonant coils of a typical coupled magnetic resonance WPT system that have mutual inductance  $M$  between them, and self-resistances,  $R_1$ ,  $R_2$  when operating at a frequency  $\omega = 2\pi f$ . For circuit theory to hold and apply the expression

as in [24], the wavelength of the electromagnetic fields should be much larger than the characteristic size of the devices used to transfer power, which is not the case here. In contrast, (19) is based only on CMT analysis and is valid for *any* two generic coupled electromagnetic resonators, regardless of wavelength or geometry [20], [21].

### III. MEASURED RESULTS AND COMPARISON TO ANALYTICAL MODEL

In this section, two resonant cavity modes are selected so that their combined regions of uniform magnetic flux density allow for seamless wireless power delivery to a receiver over large volumes of the chamber. Since no *one* resonant mode exists that has a magnetic field that is the same magnitude and direction everywhere, it is necessary to use more than one resonant mode to cover a large volume of the chamber. For experimental purposes, it is necessary to excite one mode at a time so as to provide a clear study of each mode in isolation, since they are expected to have regions of high and low efficiency that correlate with the local strength of  $B_y$  as in Fig. 2(b) and (c). The combination of the two modes, measured individually, leads to the overall demonstration of attaining high efficiencies over large volumes of the chamber when the WPT system is in full operation. In a practical system, the use of multiple modes could be accomplished by time multiplexing the excitation of each of two or more modes.

This section presents experimental data, which is compared to the analytic prediction of efficiency introduced in Section II-D. This is done by using a vector network analyzer (VNA) to measure the transfer of energy in terms of scattering parameters (or  $S$ -parameters) between the input to the cavity and a receiver. These results are used to find  $\eta_{\max}$ , the maximum possible wireless power transfer efficiency of the system. This is done as the receiver's position within the chamber is varied.

The "transmitter" here consists of the linear probe antenna, which excites a particular mode of the cavity. The linear probe excites spatially varying electromagnetic waves within the cavity that reflect off the interior walls of the structure, leading to standing waves. It is these standing waves and their magnetic fields that couple to the receiver via magnetic induction and provide power wirelessly to the receiver. The theoretical standing wave patterns for the two modes are shown in Fig. 2(b) and (c).

#### A. Experimental Methods for Wirelessly Powering Large Volumes

To experimentally validate the proposed system, a large resonant chamber has been constructed as shown in Fig. 4. The cavity has dimensions  $a = 1.52$  m,  $b = 1.42$  m, and  $d = 1.83$  m, with walls made of Aluminum. Additionally, a square-shaped single-turn coil made of copper was built for the receiver. The coil is 7.62 cm on each side [ $s = 7.62$  cm, as depicted in Fig. 4(b)]. To mount the coil at various heights within the chamber, it was affixed to a tall polyvinylchloride (PVC) pipe. Once attached to the pipe, the coil [on the pipe] was moved over an  $xy$  grid of 10  $x_o$  and 11  $y_o$  positions. The coil was affixed to the pipe at five different heights:  $z_o = 0.40$  m, 0.65 m, 0.93 m, 1.35 m, and 1.71 m, from bottom to top, respectively.

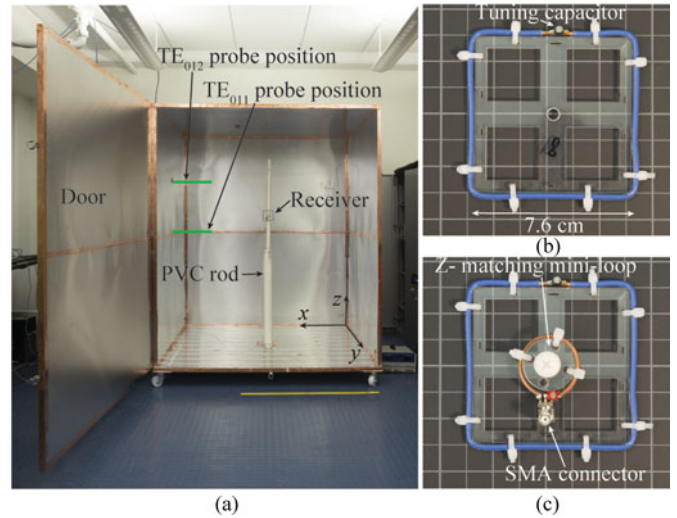


Fig. 4. (a) Picture of the experimental aluminum cavity, with yellow yard stick for scale. (b) Closeup of square-shaped copper coil receiver with tuning capacitor. (c) Closeup of coil receiver with smaller impedance matching mini-loop. The two together form a complete receiver with the mini-loop's output running back to the VNA for  $S$ -parameter measurements.

For each of the two modes, either  $TE_{011}$  or  $TE_{012}$ , a 29.53-cm-long copper linear probe antenna is used to couple into the chamber. To excite the  $TE_{011}$  mode, the probe was mounted at position  $(a, b/2, d/2)$ . To excite the  $TE_{012}$  mode, the probe was mounted at position  $(a, b/2, 3/4d)$ . These locations are specified with the coordinate system depicted in Fig. 2(a). Determining the position of the probes for the  $TE_{011}$  or  $TE_{012}$  modes was accomplished by first inspecting the regions where the electric field of the desired cavity mode was strongest [see red arrows of Fig. 2(b) and (c)]. Next, the linear probe was mounted in those regions such that it drives current down its axis (and thus electric fields) in the same direction as the desired mode. A probe mounted in this way couples strongly to the natural fields of the cavity resonator and efficiently excites the desired mode.

The experimental procedure for measuring WPT efficiency is identical for both the  $TE_{011}$  and  $TE_{012}$  modes. First, the door to the chamber is closed with port one of a VNA attached to the linear transmitter probe via a coaxial cable on the exterior of the chamber, to record  $S$ -parameters. In particular,  $S_{11}$  is recorded and used to extract the resonant frequency of the desired mode, as well as its  $Q$ -factor, using standard RF measurement techniques [25]. The measured resonant frequencies of the  $TE_{011}$  and  $TE_{012}$  modes are  $f_o = 132.76$  and 193.93 MHz, respectively. Their  $Q$ -factors are 2300 and 450, respectively.

Next, the coil is characterized in isolation (i.e., outside of the chamber). A variable capacitor is used to tune the square coil such that the  $LC$  tank resonates at the same frequency as the chamber. Its  $Q$  factor is similarly extracted and found to be approximately 300. Finally, the coil is placed in the chamber (affixed to the PVC pipe). The wireless power link formed between the linear probe's connection to the VNA port 1 and the receiver attached to port 2 can be viewed as a generic two-port network. One of the keys to high-efficiency wireless power transfer is to obtain a biconjugate impedance-matched system

[26]–[29], and the topologies of these circuits are varied and numerous [6], [30], [31].

To accomplish this impedance match, we use the following techniques: on the transmitter side, physically cutting the linear transmit probe until it was 29.53 cm long provided a good impedance match (minimum  $|S_{11}|$ ) to the chamber when the coil was inside. This was done empirically. On the receiver side, the choice of impedance matching network on the receiver is the “mini-loop” [32] topology common throughout the MQS WPT literature. Thus, the complete receiver consists of a single-turn square-shaped coil tuned to the resonant frequency of the desired mode, and a small 2.5-cm diameter circular coil (also tuned to the resonant frequency of the  $TE_{011,012}$  modes). A picture of the receiver is shown in Fig. 4(c).

Once the tuning process is complete, the receiver is mounted to the PVC pole and a coax cable was used to connect the receiver to port 2 of the VNA. Thus, the 50- $\Omega$  terminal of the VNA was the load and source impedance in these experiments. At each position of the measurement  $xy$  grid,  $S$ -parameters were recorded and the resulting  $|S_{21}|^2$  is used to determine the raw WPT efficiency (note,  $\text{Efficiency} = |S_{21}|^2$ ).

The frequency at which  $|S_{21}|^2$  reaches a maximum at a given coil location can be different from the individual resonant frequency of the chamber or coil receiver. This is due to the fact that throughout much of the chamber, the system is in the over-coupled regime and so frequency splitting of the system occurs [7]. Thus, in these experiments, approximately a 10-MHz band was considered (centered around  $f_o$  of the chamber in isolation) when finding the maximum of  $|S_{21}|^2$ . As the coil moves to each position, the frequency is scanned and the maximum  $|S_{21}|^2$  contained within that scan is recorded. The  $S$ -parameters at that frequency are then used in MATLAB’s built-in function “powergain” to compute the measured  $\eta_{\max}$ . As mentioned in Section II-D, this is the maximum power transfer efficiency assuming optimal impedance matching. This measurement is done so as to validate the analytic prediction that is based on computation of the coupling coefficient.

### B. Comparison of Measured Results to Analytical Theory

The results for the measured  $\eta_{\max}$  efficiency is plotted in Fig. 5(a)–(c). All panels present the WPT efficiency using contour plots drawn at the corresponding  $z$  level at which the receiver was positioned. Panel (a) shows the results for the  $TE_{011}$  mode, and panel (b) shows the results for the  $TE_{012}$  mode. Generally, where the magnetic flux density is high [see Fig. 2(b) and (c)], the upper bound on efficiency is seen to reach peak values of  $\sim 70$ – $80\%$ . Large volumes are covered by efficiencies of 50% or greater. On the other hand, regions where the magnetic flux density is expected to be low based on the modal field structure have efficiencies  $< 10\%$ . However, Fig. 5(a) and (b) shows that where one mode has relatively low WPT efficiency; the other generally has higher efficiency. Consequently, Fig. 5(c) then shows the result for  $\eta_{\max}$  where on a point-by-point basis, the maximum value for either the  $TE_{011}$  or  $TE_{012}$  is selected. In other words, either the  $TE_{011}$  or  $TE_{012}$  is excited individually in this experiment, but the results of (c) are obtained by taking the maximum value obtained between the experiments of (a) and

(b). By using two modes (either simultaneously or time multiplexed), high-efficiency WPT can be provided to a receiver over large volumes of the chamber.

The measured efficiency plots of Fig. 5(a)–(c) match well the predicted values shown in Fig. 5(d)–(e). Panels (d) and (e) are theoretical plots produced when using the analytic value of  $\kappa$  (19), along with the measured  $Q$  factors of chamber and coil, to predict the efficiencies obtainable when the system is biconjugate impedance matched. Coils placed in different orientations would yield similar results if corresponding modes of the chamber are excited such that the modes have appropriately directed magnetic flux. By the symmetry of the problem, modes similar to the  $TE_{011}$  and  $TE_{012}$  modes can be used for exciting a coil lying in other planes and thus can deliver power to a coil with almost any orientation and position within the chamber. Finally, note that this work has so far not considered any receiver optimization. Receiver coils with larger diameters, more turns, or lower material loss would result in even higher efficiencies.

Finally, we note that the proposed system here only uses one mode at a time to achieve high efficiency over large volumes. For example, if the receiver is in a place where the efficiency of the  $TE_{011}$  mode is high for a given receiver orientation and position, then that mode is used. On the other hand, if the receiver has an orientation and position that favors the  $TE_{012}$  mode, then that mode would be solely excited. Practically speaking, this system could be realized by scanning frequency rapidly across the band containing all potential modes, and then choosing to solely excite which frequency (and therefore mode) produces the strongest minimum in the  $|S_{11}|$  parameter (measured with a directional coupler), compared to when there is no receiver inside. Finally, to ensure high efficiency, adaptive impedance-matching techniques on the source and receiver ends can be used to fine tune the system.

## IV. EXPERIMENTAL DEMONSTRATION OF CAVITY MODE ENABLED WPT

Due to the uniformity of the magnetic flux density over certain regions of the chamber for a given mode, there exists not only the opportunity to power one device over large volumes, but to also provide power to many devices simultaneously. In this section, high power transfer to a device in multiple locations will be detailed. Then, an experiment that demonstrates WPT to multiple receivers connected to individual loads will be presented. Finally, a practical example of powering a consumer electronic device (cell phone) is shown.

### A. Power Transfer to a Device in Multiple Locations

In Section III, measurements were taken to experimentally determine the upper bounds on the WPT efficiency so that it could be compared to our analytical model. In this section, an impedance matching network is added to the receiver so that the raw power transfer efficiency can be measured for the  $TE_{012}$  mode for various locations in the chamber. This is accomplished by measuring the  $S$ -parameters with a VNA, for the receiver located on the  $x, y, z$  grid previously described.

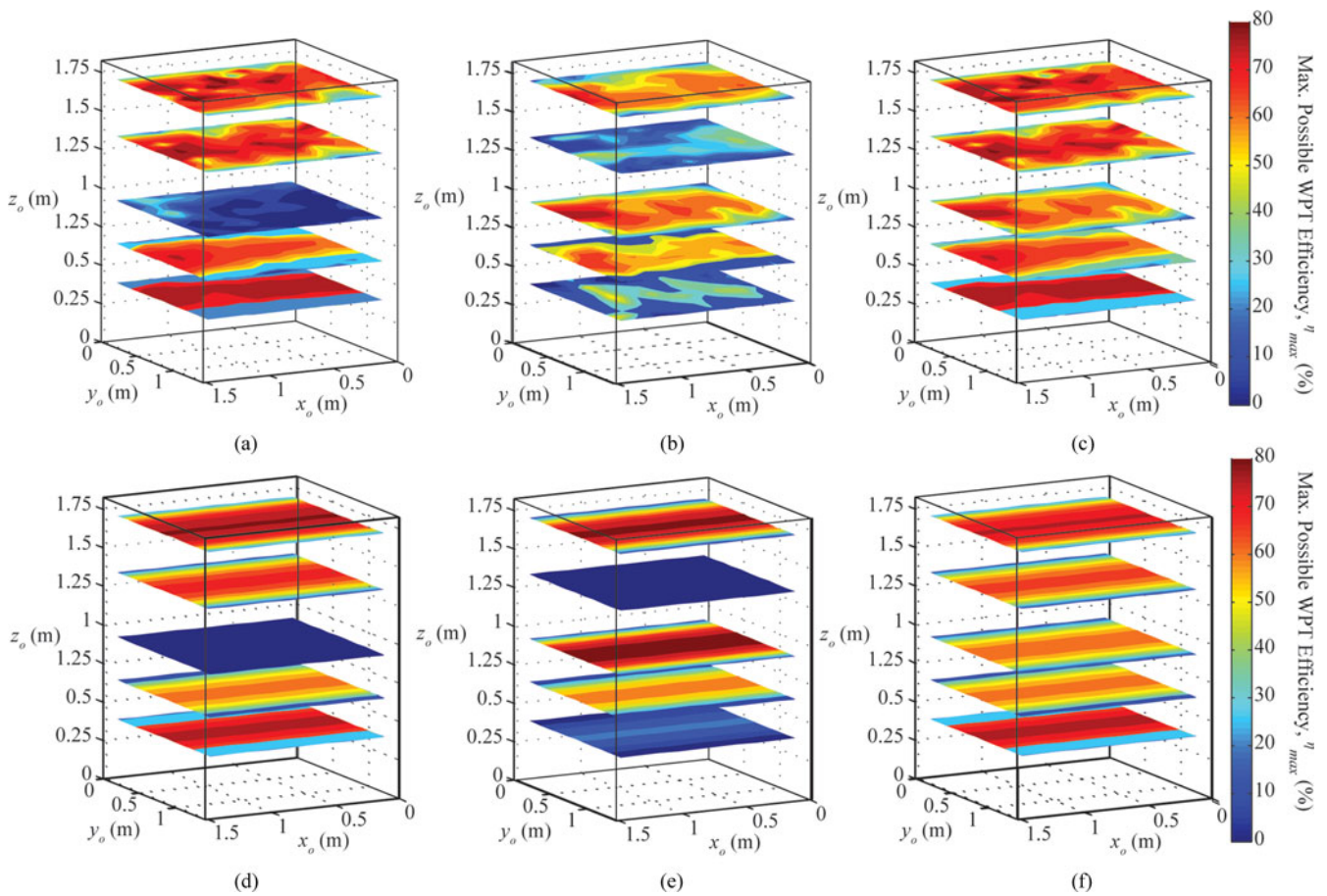


Fig. 5. Upper bound on possible WPT efficiency,  $\eta_{\max}$ , at varied  $z$  heights as the receiver is scanned across the  $xy$  plane at each height. Panel (a) is  $\eta_{\max}$  for the  $TE_{011}$  mode, (b) is for the  $TE_{012}$  mode, and (c) is the composite formed by taking the maximum efficiency obtained in either (a) or (b) at each point. For comparison to the analytic approach, (d)–(f) are the predicted upper bound on efficiency,  $\eta_{\max}$ , from using (19) over the  $xy$  plane at different  $z_o$  heights of the receiver coil.

The raw WPT efficiency is obtained from the power transfer coefficient,  $|S_{21}|^2$  (i.e., Efficiency =  $|S_{21}|^2$ ). This data are shown in Fig. 6(a) and (b). In panel (a), the result shown is the power transfer coefficient,  $|S_{21}|^2$ , when the receiver is tuned and moved over the same five  $z$ -levels as in Section III. Importantly, the results are for a receiver that was tuned only *once* and then moved within the chamber. Even without dynamically retuning the receiver as its position within the chamber varies, the power transfer efficiencies exceed 50% in many regions within the chamber. One of the strengths of cavity mode enabled WPT is that a receiver tuned once can efficiently receive power whenever it is somewhere in the chamber where the magnetic flux density is relatively high. The raw  $|S_{21}|^2$  WPT efficiencies in Fig. 6(a) are within 10–20% of the maximum possible efficiencies  $\eta_{\max}$  in Fig. 5(b). If a dynamic impedance matching network is used to retune the receiver at each location, the results for  $|S_{21}|^2$  would be even closer to the upper bounds on efficiency in Fig. 5(b).

These results will be important in the next section, since the multiple receiver experiment is conducted over the middle  $xy$  plane of the chamber. In this case, Fig. 6(a) clearly shows that efficiencies of about 50% or greater can be expected to any one

device in this plane. To further corroborate this result, Fig. 6(b) is the case when the receiver is located in the middle of the chamber. It shows a good impedance match as evidenced by the minima in  $S_{11}$  and  $S_{22}$  and relatively high power transfer efficiency of around 60%.

### B. Powering Multiple Devices Simultaneously

Here, attention now turns to the powering of multiple devices simultaneously. For this experiment, the  $TE_{012}$  mode is chosen as in Section IV-A since it has a region of  $y$ -directed magnetic flux density throughout the middle of the chamber, which is a convenient place to set multiple receivers. If the receivers were desired to be positioned near the bottom or top of the chamber, then the  $TE_{012}$  would likely be a better choice. Ultimately, a designer should select the cavity mode that has strong magnetic flux crossing the surface of the receivers, given the receivers' fixed position and orientation. The transmitter is the same as in Section III, a 29.53-cm-long, copper, linear probe. Each receiver is a square-shaped copper coil of 7.62 cm on each side. For the impedance-matching element and load, a circular printed circuit board mini-loop was used, 3.8 cm in diameter, that attached

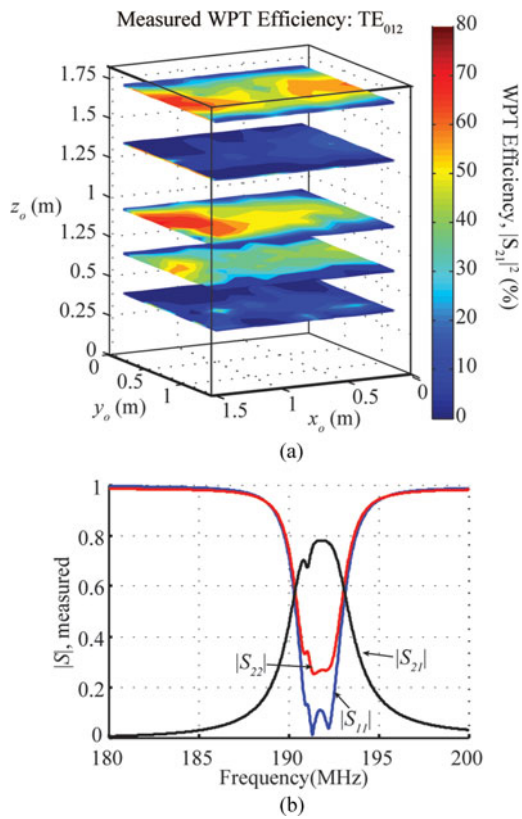


Fig. 6. (a) Wireless power transfer efficiency (Efficiency =  $|S_{21}|^2$ ) for a receiver impedance matched near the center of the chamber to the  $TE_{012}$  mode and then moved throughout the chamber. Even though the receiver is not dynamically retuned at each point, high WPT efficiencies are still obtained. (b)  $S$ -parameters versus frequency between chamber input port and receiver. The data in (b) are single point in (a):  $(x_o, y_o, z_o) = (a/2, b/2, d/2)$ . The peak in  $|S_{21}|$  indicates WPT efficiency of around 60% at this position.

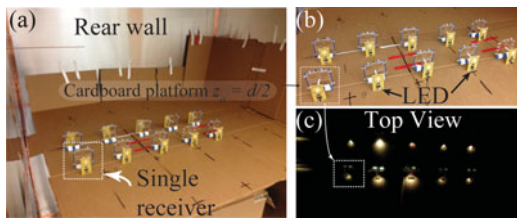


Fig. 7. (a) Photo of ten WPT receivers attached to half wave rectifiers that power white LEDs. (b) Zoomed-in view of the same setup. (c) Photo of the ten LEDs powered simultaneously and at a single operating frequency.

to a half-wave rectifier, connected to an LED (Mfg. part no. MLESWT-A1-000-0003E5). A picture of the square coil and the loop connected to rectifier and LED is shown in Fig. 7(a). Together, the square coil and PCB loop/rectifier combination form what will be referred to as the receiver.

To mount the receivers, a cardboard platform was constructed so that the coils could be positioned in the  $xy$  plane at a height of  $z_o = d/2 = 91$  cm [i.e., half way between the floor and ceiling of the chamber, as noted in Fig. 7(a)]. In this case, the resonant frequency of the receivers was tuned to was  $f_o = 191.65$  MHz.

After the tuning process was completed, and the efficiencies of WPT to the receivers at various locations had been measured, the linear probe antenna was attached to the output of a commercially available AR Modular model 75A400 power amplifier (PA). The ten receivers were then positioned within the chamber and the power amplifier and signal generator turned ON (with the door to the chamber closed). When the receivers are positioned within the chamber, it is necessary to have them about 1 coil diameter apart so that they effectively act independently and couple only to the chamber [7], and not strongly to each other. Receiver coupling to each other significantly complicates the analysis, but does not mean power cannot be transferred to devices closer than 1 coil diameter.

Next, the power amplifier's input was connected to a signal generator set to output 193.67 MHz, which was the frequency at which all LEDs glowed with similar brightness. This frequency was determined by fine tuning the frequency around the original  $f_o = 191.65$  MHz. Other frequencies powered some LEDs and not others, but not all at once. This would be the frequency where all devices are relatively well impedance matched to the source [33]. Fig. 7(a) shows an image of the ten receivers positioned within the chamber. Panel (c) of the same figure shows the LEDs glowing wirelessly within the chamber once the power had been switched ON. This was accomplished at a *single tone* input to the PA, and no frequency sweeping was necessary once 193.67 MHz was identified as optimal for simultaneous operation of the ten LEDs.

Since the devices are identical, an estimate of the power transfer efficiency to all devices can be obtained by taking the power transfer efficiency to *one* device, and dividing it by the number of devices. As was shown in Fig. 6(a) and (b) of the last subsection, 50–60% efficiency can be obtained to one device in similar positions; thus, from this  $S_{21}$  measurement of one device, it can be concluded that each receiver obtains around 5% of the total power, while the group of ten devices received a total of 50% of the total RF power. To simultaneously keep all devices lit at the same resonant frequency, the order of 8 W of power had to be provided from the output of the power amplifier to further compensate for the inefficiency of the rectifier. With rectifiers of approximately 40–50% efficiency, this leaves the percent of total power received by each LED of around 2–3%. The RF-DC efficiency from input to all ten devices is consequently 20–30%. In this experiment, no optimization of the rectifier was performed: thus, overall efficiency could be greatly improved with further design refinement. Nonetheless, the goal of powering many devices simultaneously using a cavity resonator is demonstrated.

### C. Wireless Powering of a Consumer Electronic Device

In this last subsection, the practical utility of cavity mode enabled wireless power transfer is demonstrated by wirelessly recharging a cellular telephone. For this demonstration, the same setup as Section IV was used, and the excitation of the  $TE_{012}$  mode was used to deliver power to the receiver within. The only difference is that instead of an LED load, the half-wave rectifier is followed by a power management board so that the appropriate voltage and current can be regulated at the input to

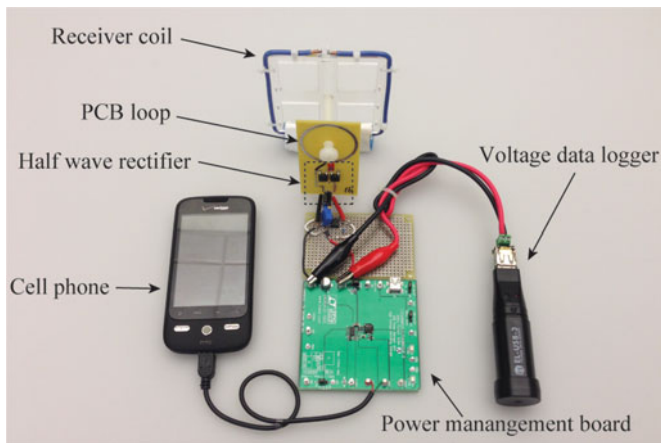


Fig. 8. Picture of the receiver and charging circuit for wirelessly charging a cell phone in the chamber. The receiver is positioned at the middle of the chamber. A voltage data logger is connected to the output of the rectifier to monitor the voltage as the RF input to the chamber is turned ON and OFF.

the cell phone battery, the load. A closeup of the receiver and cell phone as positioned within the chamber is shown in Fig. 8.

In this experiment, the receiver is positioned at the center of the chamber, so the reflection coefficients and WPT efficiency are given by Fig. 6(b), since that data were taken for a receiver at the same position. Thus, the WPT efficiency for this experiment is around 60%.

The power amplifier that drives the linear antenna is adjusted such that when the system is running, it drives approximately 1 W of power into the chamber. To monitor the output voltage of the receiver circuit while attached to the cell phone, a voltage data logger is used. Fig. 9(a) shows the difference in the magnitude of the reflection coefficient,  $|S_{11}|$ , between when the receiver/phone is inside the chamber and when it is not. This measurement is taken by monitoring the forward and reflected power ports on a directional coupler attached to the output of the power amplifier. The figure shows the influence of the resonant receiver via the pronounced decrease in the minimum of  $|S_{11}|$  when the receiver is inside, compared to when it is not. This shows that the chamber is well coupled to the resonant receiver inside.

Fig. 9(b) shows the voltage at the output of the rectifier versus time for a 120-s period before and after the power amplifier input to the chamber is turned on. The figure shows that after the power is turned on the voltage rises to 5.6 V. The initial sharp spike at 240 s is when a sweep of the frequency of the source is first performed across the frequencies of Fig. 9(a). By first recording  $|S_{11}|$  across frequency, the optimal operating frequency can then be selected by choosing where  $|S_{11}|$  is minimum. After identifying this frequency, the system input is held there for the 120 s interval where Fig. 9(b) has a constant 5.6 V.

Finally, as expected, when the input to the PA was turned ON, the phone lit up and began charging. Thus, a practical cavity mode enabled wireless power transfer system has been demonstrated with regard to its ability to power consumer electronic devices, a common application across all methods of wireless power transfer.

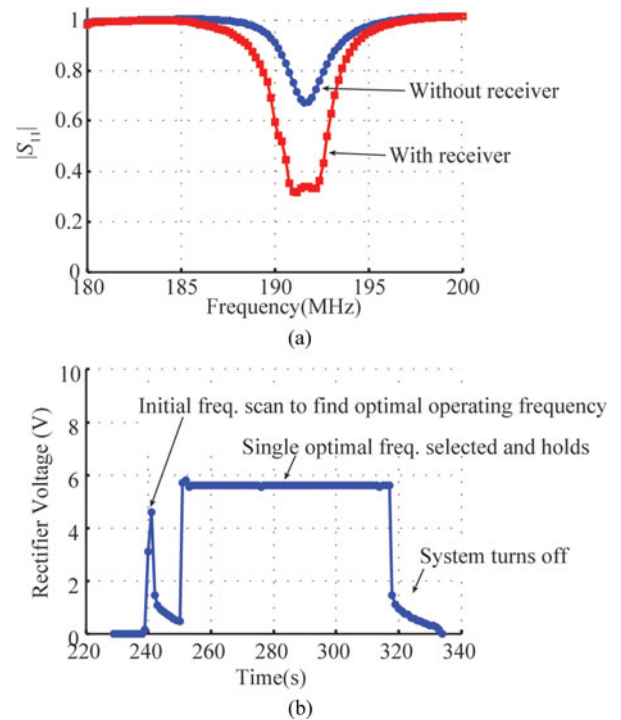


Fig. 9. (a)  $|S_{11}|$  data as measured by monitoring the forward and reflected power ports of a directional coupler attached to the PA feeding the chamber. (b) Voltage versus time at the output of the half wave rectifier of the receiver. The initial sharp peak at 240 s is due to the frequency sweep performed to identify optimal operating frequency, where the data in (a) is quickly collected. The frequency at which  $|S_{11}|$  is minimum in (a) is then selected and held, after which the rectifier voltage stabilizes at 5.6 V.

## V. CONCLUSION

In this paper, we demonstrated the viability of an unexplored form of wireless power transfer based on the resonant cavity modes of an enclosed structure. The fundamental underpinning physics have been presented using CMT. In particular, an expression for the coupling coefficient between an electromagnetic cavity resonator and a small receiver contained within is derived. The coupling coefficient is then used, along with  $Q$  factors of the cavity and receiver, to predict an upper bound on the WPT efficiency for a coil located at any point within the cavity. The analytic prediction compared well with measured results for power transfer efficiency. By using the intuition gained from this analysis, a demonstration revealed that by using one or more resonant modes of the cavity resonator, it is possible to efficiently deliver power to large volumes of the enclosed structure a receiver placed inside.

Since large volumes of the chamber can be reached at high WPT efficiency when powering one receiver, the topology of that system is extended so that it is capable of delivering power to many devices simultaneously. In this study, multiple LEDs attached to receiver coils were lit simultaneously. Finally, the practical utility of the proposed system was demonstrated by delivering power to an actual consumer electronic device—a cell phone. These initial results show that resonant cavity mode-based wireless power transfer has the potential to enable a wide

variety of new applications in the scientific, medical, and industrial fields where simultaneous charging of multiple devices anywhere in an enclosed 3-D structure is needed.

#### REFERENCES

- [1] S. Lee, J. Huh, C. Park, N. Choi, G. Cho, and C. Rim, "On-line electric vehicle using inductive power transfer system," in *Proc. IEEE Energy Convers. Congr. Expo.*, Sep. 12–16, 2010, pp. 1598–1601.
- [2] A. K. RamRakhyani, S. Mirabbasi, and M. Chiao, "Design and optimization of resonance-based efficient wireless power delivery systems for biomedical implants," *IEEE Trans. Biomed. Circuits Syst.*, vol. 5, no. 1, pp. 48–63, Feb. 2011.
- [3] B. L. Cannon, J. F. Hoburg, D. D. Stancil, and S. C. Goldstein, "Magnetic resonant coupling as a potential means for wireless power transfer to multiple small receivers," *IEEE Trans. Power Electron.*, vol. 24, no. 7, pp. 1819–1825, Jul. 2009.
- [4] D. W. Baarman, "Portable inductive power station," U.S. Patent 7 462 951, Dec. 9, 2008.
- [5] A. P. Sample, B. H. Waters, S. T. Wisdom, and J. R. Smith, "Enabling seamless wireless power delivery in dynamic environments," *Proc. IEEE*, vol. 101, no. 6, pp. 1343–1358, Jun. 2013.
- [6] A. Kurs, A. Karalis, R. Moffatt, J. D. Joannopoulos, P. Fisher, and M. Soljacic, "Wireless power transfer via strongly coupled magnetic resonances," *Science*, vol. 317, no. 5834, pp. 83–86, Jul. 2007.
- [7] A. Sample, D. Meyer, and J. Smith, "Analysis, experimental results, and range adaptation of magnetically coupled resonators for wireless power transfer," *IEEE Trans. Ind. Electron.*, vol. 58, no. 2, pp. 544–554, Feb. 2011.
- [8] W. X. Zhong, C. K. Lee, and S. Y. Hui, "Wireless power domino-resonator systems with noncoaxial axes and circular structures," *IEEE Trans. Power Electron.*, vol. 27, no. 11, pp. 4750–4762, Nov. 2012.
- [9] C. K. Lee, W. X. Zhong, and S. Y. Hui, "Effects of magnetic coupling of nonadjacent resonators on wireless power domino-resonator systems," *IEEE Trans. Power Electron.*, vol. 27, no. 4, pp. 1905–1916, Apr. 2012.
- [10] T. Nguyen, S. Li, W. Li, and C. C. Mi, "Feasibility study on bipolar pads for efficient wireless power chargers," in *Proc. 29th Annu. IEEE Appl. Power Electron. Conf. Expo.*, Mar. 16–20, 2014, pp. 1676–1682.
- [11] M. Budhia, G. A. Covic, and J. T. Boys, "Design and optimization of circular magnetic structures for lumped inductive power transfer systems," *IEEE Trans. Power Electron.*, vol. 26, no. 11, pp. 3096–3108, Nov. 2011.
- [12] M. H. Mickle, C. C. Capelli, H. Swift, L. Matts, M. Mi, and C. E. Greene, "Recharging method and apparatus," U.S. Patent 7 373 133, May 13, 2008.
- [13] Z. Hatem, T. H. Wilson, and K. K. Clark, "Systems and methods for optimally delivering pulsed wireless power," U.S. Patent 14/171 750.
- [14] W. C. Brown, "The history of power transmission by radio waves," *IEEE Trans. Microw. Theory Techn.*, vol. MTT-32, no. 9, pp. 1230–1242, Sep. 1984.
- [15] M. J. Chabalko and A. P. Sample, "Resonant cavity mode enabled wireless power transfer," *Appl. Phys. Lett.*, vol. 105, no. 24, p. 243902, 2014.
- [16] D. M. Pozar, *Microwave Engineering*. New York, NY, USA: Wiley, 2009, ch. 6.
- [17] D. K. Cheng, *Fundamentals of Engineering Electromagnetics*. Englewood Cliffs, NJ, USA: Prentice-Hall, 1993.
- [18] J. D. Jackson, *Classical Electrodynamics*, 3rd ed. Hoboken, NJ, USA: Wiley, 1999.
- [19] A. Bodrov and S. Sul, *Wireless Power Transfer—Principles and Engineering Explorations*. Rijeka, Croatia: InTech, 2012, ch. 2.
- [20] H. Haus, *Waves and Fields in Optoelectronics*. Englewood Cliffs, NJ: Prentice-Hall, 1984, ch. 7.
- [21] H. Haus and W. Huang, "Coupled-mode theory," *Proc. IEEE*, vol. 79, no. 10, pp. 1505–1518, Oct. 1991.
- [22] D. A. Hill, *Electromagnetic Fields in Cavities: Deterministic and Statistical Theories*, vol. 35, New York, NY, USA: Wiley, 2009, chs. 1–3.
- [23] M. Gupta, "Power gain in feedback amplifiers, a classic revisited," *IEEE Trans. Microw. Theory Techn.*, vol. 40, no. 5, pp. 864–879, May 1992.
- [24] Y. Zhang, Z. Zhao, and K. Chen, "Frequency decrease analysis of resonant wireless power transfer," *IEEE Trans. Power Electron.*, vol. 29, no. 3, pp. 1058–1063, Mar. 2014.
- [25] D. Kajfez and E. J. Hwan, "Q factor measurements with network analyzer," *IEEE Trans. Microw. Theory Techn.*, vol. MTT-32, no. 7, pp. 666–670, Jul. 1984.
- [26] M. Zargham and P. G. Gulak, "Maximum achievable efficiency in near-field coupled power-transfer systems," *IEEE Trans. Biomed. Circuits Syst.*, vol. 6, no. 3, pp. 228–245, Jun. 2012.
- [27] M. Chabalko, E. Alarcon, E. Bou, and D. S. Ricketts, "Optimization of WPT efficiency using a conjugate load in non-impedance matched systems," in *Proc. IEEE Antennas Propag. Symp.*, 2014, pp. 645–646.
- [28] E. Bou, R. Sedwick, and E. Alarcon, "Maximizing efficiency through impedance matching from a circuit-centric model of non-radiative resonant wireless power transfer," in *Proc. IEEE Int. Symp. Circuits Syst.*, 2013, pp. 29–32.
- [29] Z. N. Low, R. A. Chinga, R. Tseng, and J. Lin, "Design and test of a high-power high-efficiency loosely coupled planar wireless power transfer system," *IEEE Trans. Ind. Electron.*, vol. 56, no. 5, pp. 1801–1812, May 2009.
- [30] H. H. Wu, G. A. Covic, J. T. Boys, and D. J. Robertson, "A series-tuned inductive-power-transfer pickup with a controllable AC-voltage output," *IEEE Trans. Power Electron.*, vol. 26, no. 1, pp. 98–109, Jan. 2011.
- [31] N. D. Donaldson and T. A. Perkins, "Analysis of resonant coupled coils in the design of radio frequency transcutaneous links," *Med. Biol. Eng. Comput.*, vol. 21, no. 5, pp. 612–627, Sep. 1983.
- [32] D. S. Ricketts, M. J. Chabalko, and A. Hillenius, "Experimental demonstration of the equivalence of inductive and strongly coupled magnetic resonance wireless power transfer," *Appl. Phys. Lett.*, vol. 102.5, p. 053904, 2013.
- [33] D. S. Ricketts, and M. J. Chabalko, "On the efficient wireless power transfer in resonant multi-receiver systems," in *Proc. IEEE Int. Symp. Circuits Syst.*, May 19–23, 2013, pp. 2779–2782.



**Matthew J. Chabalko** received the B.S. degree in electrical engineering from Lehigh University, Bethlehem, PA, USA, in 2006, and the M.S. and Ph.D. degrees from Carnegie Mellon University, Pittsburgh, PA, in 2008 and 2012, respectively.

He is currently an Associate Research Scientist at Disney Research, Pittsburgh. His Ph.D. work focused on analysis and design of nano-optic, near-field transducers for heat-assisted magnetic recording. Since then, his work has focused mainly on magnetoquasistatic and other types of wireless power transfer.

His general research interests include optics, near-field imaging, metamaterials, wireless power transfer, and electromagnetic theory.



**Alanson P. Sample** (M'03) received the B.S., M.S., and Ph.D. degrees in electrical engineering from the University of Washington, Seattle, WA, USA, in 2005, 2008, and June 2011, respectively.

He is currently a Research Scientist at Disney Research, Pittsburgh, PA, USA, where he leads the Wireless Systems group. Prior to joining Disney, he was a Postdoctoral Researcher in the Department of Computer Science and Engineering, University of Washington. There, he developed methods of wirelessly powering implanted heart pumps, known as LVADs.

Throughout his graduate studies, he worked full time at Intel Research, Seattle, where he published several articles and patents on the use of magnetically coupled resonators for wireless power delivery, as well as RFID, and ambient RF energy harvesting. He was one of the key contributors to the Wireless Identification and Sensing Platform, which was open-sourced in 2009 as part of Intel's WISP Challenge. His research interests lie broadly in the areas of wireless communication, RF and analog circuit design, embedded systems, and novel sensors.